NeuroImage 51 (2010) 629–641

Contents lists available at ScienceDirect

NeuroImage

journal homepage: www.elsevier.com/locate/ynimg

A generalized method to estimate waveforms common across trials from EEGs

Yusuke Takeda [a,*], Masa-aki Sato [a], Kentaro Yamanaka [b], Daichi Nozaki [c], Yoshiharu Yamamoto [c]

[a] ATR Computational Neuroscience Laboratories, 2-2-2 Hikaridai, Keihanna Science City, Kyoto 619-0288, Japan
[b] Department of Health Design, Showa Women's University, 1-7 Taishido, Setagaya-ku, Tokyo 154-8533, Japan
[c] Educational Physiology Laboratory, Graduate School of Education, The University of Tokyo, 7-3-1 Hongo, Bunkyo-ku, Tokyo 113-0033, Japan

ARTICLE INFO

Article history:
Received 29 April 2009
Revised 24 December 2009
Accepted 2 February 2010
Available online 10 February 2010

Keywords:
Electroencephalography (EEG)
EEG waveforms common across trials
Go/NoGo task

ABSTRACT

We propose a generalized method to estimate waveforms common across trials from electroencephalographic (EEG) data. From single/multi-channel EEGs, the proposed method estimates the number of waveforms common across trials, their delays in individual trials, and all of the waveforms. After verifying the performance of this method by a number of simulation tests with artificial EEGs, we apply it to EEGs during a Go/NoGo task. This method can be used in general situations where the number and the delays of EEG waveforms common across trials are unknown.

© 2010 Elsevier Inc. All rights reserved.

Introduction

In many electroencephalographic (EEG) studies, EEG waveforms common across trials have been estimated by averaging EEG epochs across trials. For example, evoked potentials, such as visual evoked potentials (VEPs), are estimated by averaging EEG epochs that are triggered on visual stimulus onsets. When waveforms temporally overlap, however, the averaging procedure cannot estimate exact waveforms because they are mutually contaminated (Kok, 1988; Takeda et al., 2008a; Verleger, 1988). Further, when the delays of waveforms are variable and unknown, the averaging procedure cannot be used (Takeda et al., 2008b; Tallon-Baudry and Bertrand, 1999).

Recently, we proposed two methods that overcome those limitations (Takeda et al., 2008a; Takeda et al., 2008b). These two methods assume that two waveforms common across trials exist in an EEG epoch and estimate them from single-channel EEG epochs. One method is used when the delays of two waveforms are given (Takeda et al., 2008a). By this method, we obtain pure waveforms that are not contaminated with each other from EEGs during stimulus–response tasks, in which the delays of two waveforms are given from stimulus and response onsets. The other method is used when the delays of a waveform are not given (Takeda et al., 2008b). By this method, we can obtain the delays as well as the pure waveforms from EEGs during covert response tasks, such as decision-making tasks.

However, these methods lack versatility. In particular, the validity of the assumption, the existence of two EEG waveforms common across trials, is not always guaranteed. Generally, the total number of waveforms is unknown. It is possible that three or more waveforms exist. In fact, the study of Verleger et al. (2005) is suggestive of three waveforms in EEGs during Go trials of a Go/NoGo task: a stimulus-locked waveform, a response-locked waveform, and a waveform time-locked to neither stimulus nor motor response onsets. In such a case, applying the above methods is inappropriate. On the other hand, the previous methods use only single-channel EEGs. While this property is an advantage when only single-channel EEGs are available, it sometimes becomes a disadvantage when multi-channel EEGs are available because using all available EEGs may provide more information than just using a small portion of it. To investigate various types of EEGs in detail, we need a more general method that can deal with an unknown number of waveforms and multi-channel EEGs.

In this paper, we propose a generalized method to estimate EEG waveforms common across trials. From single/multi-channel EEGs, the proposed method estimates the number of waveforms common across trials, their delays in individual trials, and all of the waveforms. We examine the performance of this method by a number of simulation tests with artificial EEGs. Then as an example, we apply this method to EEGs during a Go/NoGo task.

Methods

Proposed method to estimate waveforms common across trials

Assumption and purpose

An EEG epoch of a channel, which is assumed to consist of waveforms common across trials and noise, is expressed by

$$y_n^{(ch)}(t) = \sum_{k=1}^{K} s_k^{(ch)}\left(t - \tau_{n,k}\right) + v_n^{(ch)}(t) \tag{1}$$
$$(t = 0,\cdots,T-1; n = 1,\cdots,N; ch = 1,\cdots,CH),$$

* Corresponding author. Fax: +81 774 95 1259.
E-mail address: takeda@atr.jp (Y. Takeda).

1053-8119/$ – see front matter © 2010 Elsevier Inc. All rights reserved.
doi:10.1016/j.neuroimage.2010.02.002

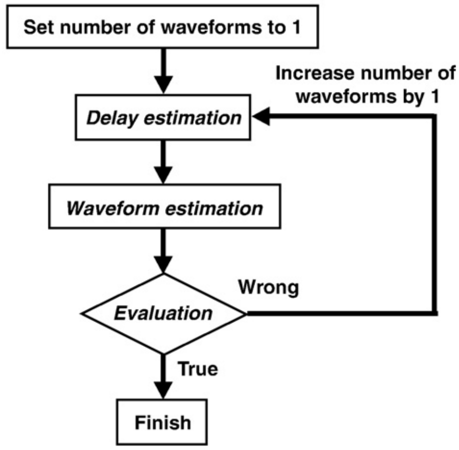

Fig. 1. Flowchart to estimate number of waveforms common across trials, their delays in individual trials, and all of the waveforms.

where $y_n^{(ch)}(t)$: observed EEG epoch of channel *ch* in trial *n*, $s_k^{(ch)}(t)$: *k*-th waveform of channel *ch*, $\tau_{n,k}$: delay of $s_k^{(ch)}(t)$ in trial *n*, $v_n^{(ch)}(t)$: noise of channel *ch* in trial *n*, and *K*: number of waveforms. Noise $v_n^{(ch)}(t)$ is assumed to be a stationary process.

For simplicity, we rewrite Eq. (1) as a matrix representation in the Fourier domain as below. By taking the discrete Fourier transform of Eq. (1), we obtain

$$Y_n^{(ch)}(\omega)=\sum_{k=1}^{K}\exp\left(-i2\pi\omega\tau_{n,k}/T\right)S_k^{(ch)}(\omega)+V_n^{(ch)}(\omega)(\omega=0,\cdots,T-1), \tag{2}$$

where $Y_n^{(ch)}(\omega)$, $S_k^{(ch)}(\omega)$, and $V_n^{(ch)}(\omega)$: the discrete Fourier transforms of $y_n^{(ch)}(t)$, $s_k^{(ch)}(t)$, and $v_n^{(ch)}(t)$, respectively. Eq. (2) is rewritten as

$$\mathbf{Y}^{(ch)}(\omega)=\mathbf{E}(\omega,\tau)\mathbf{S}^{(ch)}(\omega)+\mathbf{V}^{(ch)}(\omega), \tag{3}$$

where

$$\mathbf{Y}^{(ch)}(\omega)=\left[Y_1^{(ch)}(\omega),\cdots,Y_N^{(ch)}(\omega)\right]^T,$$

$$\mathbf{E}(\omega,\tau)=\begin{bmatrix}\exp\left(-i2\pi\omega\tau_{1,1}/T\right) & \cdots & \exp\left(-i2\pi\omega\tau_{1,K}/T\right)\\ \vdots & \ddots & \vdots\\ \exp\left(-i2\pi\omega\tau_{N,1}/T\right) & \cdots & \exp\left(-i2\pi\omega\tau_{N,K}/T\right)\end{bmatrix},$$

$$\tau=\tau_{n,k}(n=1,\cdots,N;k=1,\cdots,K),$$

$$\mathbf{S}^{(ch)}(\omega)=\left[S_1^{(ch)}(\omega),\cdots,S_K^{(ch)}(\omega)\right]^T,$$

and

$$\mathbf{V}^{(ch)}(\omega)=\left[V_1^{(ch)}(\omega),\cdots,V_N^{(ch)}(\omega)\right]^T.$$

The purpose of the proposed method is to obtain $\hat{\mathbf{S}}^{(ch)}(\omega)\hat{\tau}$ and $\hat{K}$ only from $\mathbf{Y}^{(ch)}(\omega)$, where $\hat{\mathbf{S}}^{(ch)}(\omega)$: the estimated $\mathbf{S}^{(ch)}(\omega)$,$\hat{\tau}$: the estimated τ, and $\hat{K}$: the estimated *K*.

Overview of procedure for obtaining $\hat{\mathbf{S}}^{(ch)}(\omega)$,$\hat{\tau}$ and $\hat{K}$

The proposed method consists of three steps: *Delay estimation*, *Waveform estimation*, and *Evaluation*, which are consecutively repeated as shown in Fig. 1. At the beginning of the procedure, we set *K* to 1. In the *Delay estimation* step, we obtain $\hat{\tau}$ using preset *K*. In the *Waveform estimation* step, we obtain $\hat{\mathbf{S}}^{(ch)}(\omega)$ using $\hat{\tau}$ and preset *K*. In the *Evaluation* step, we evaluate whether preset *K* is true using $\hat{\mathbf{S}}^{(ch)}(\omega)$ and $\hat{\tau}$. If preset *K* is evaluated as wrong, we return to the *Delay estimation* step by increasing preset *K* by 1. By repeating this procedure until preset *K* is evaluated as true, we can simultaneously obtain $\hat{\mathbf{S}}^{(ch)}(\omega)$,$\hat{\tau}$, and $\hat{K}$.

The *Evaluation* procedure is based on the results of *Delay estimation* and *Waveform estimation*. The procedure of *Delay estimation* is based on that of *Waveform estimation*. Therefore, we describe these steps in the following order: *Waveform estimation*, *Delay estimation*, and *Evaluation*.

Waveform estimation

In this step, we estimate $\mathbf{S}^{(ch)}(\omega)$ from $\mathbf{Y}^{(ch)}(\omega)$ when τ and *K* are given.

In the least squares method, estimated $\mathbf{S}^{(ch)}(\omega)$ is expressed by

$$\hat{\mathbf{S}}^{(ch)}(\omega)=\underset{\mathbf{S}^{(ch)}(\omega)}{\operatorname{argmin}}\ ||\mathbf{Y}^{(ch)}(\omega)-\mathbf{E}(\omega,\tau)\mathbf{S}^{(ch)}(\omega)||^2,$$

where $\underset{x}{\operatorname{argmin}}\cdots$ represents *x* that minimizes ⋯ and || ⋯ || represents the norm of ⋯. By solving

$$\frac{\partial||\mathbf{Y}^{(ch)}(\omega)-\mathbf{E}(\omega,\tau)\mathbf{S}^{(ch)}(\omega)||^2}{\partial\mathbf{S}^{(ch)}(\omega)}=0,$$

we obtain

$$\hat{\mathbf{S}}^{(ch)}(\omega)=\left[\mathbf{E}(\omega,\tau)^T\mathbf{E}(\omega,\tau)\right]^{-1}\mathbf{E}(\omega,\tau)^T\mathbf{Y}^{(ch)}(\omega). \tag{4}$$

When $\omega=0$, all of the values in $\mathbf{E}(\omega,\tau)$ become 1, and $\mathbf{E}(\omega,\tau)^T\mathbf{E}(\omega,\tau)$ becomes singular. This corresponds to the fact that arbitrary constants can be added to $\hat{s}_k^{(ch)}(t)$. Therefore, we set the time average of $\hat{s}_k^{(ch)}(t)$ to be 0 by

$$\hat{\mathbf{S}}^{(ch)}(\omega)=\begin{cases}0 & \omega=0\\ \left[\mathbf{E}(\omega,\tau)^T\mathbf{E}(\omega,\tau)\right]^{-1}\mathbf{E}(\omega,\tau)^T\mathbf{Y}^{(ch)}(\omega) & \omega\neq0\end{cases}. \tag{5}$$

We can obtain $\hat{s}_k^{(ch)}(t)$ by taking the inverse discrete Fourier transform of $\hat{\mathbf{S}}^{(ch)}(\omega)$.

Delay estimation

In this step, we estimate τ from $\mathbf{Y}^{(ch)}(\omega)$ when *K* is given.

In the least squares method, estimated τ is expressed by

$$\hat{\tau}=\underset{\tau}{\operatorname{argmin}}\sum_{ch=1}^{CH}\sum_{\omega=1}^{T/2}||\mathbf{Y}^{(ch)}(\omega)-\mathbf{E}(\omega,\tau)\mathbf{S}^{(ch)}(\omega)||^2. \tag{6}$$

In this equation, since $\mathbf{S}^{(ch)}(\omega)$ is neither known nor determined by τ, we replace it by $\hat{\mathbf{S}}^{(ch)}(\omega)$ in Eq. (5), which is the least squares solution of $\mathbf{S}^{(ch)}(\omega)$ determined by τ. Then Eq. (6) is rewritten as

$$\hat{\tau}=\underset{\tau}{\operatorname{argmin}}\sum_{ch=1}^{CH}\sum_{\omega=1}^{T/2}||\mathbf{Y}^{(ch)}(\omega)-\mathbf{E}(\omega,\tau)\left[\mathbf{E}(\omega,\tau)^T\mathbf{E}(\omega,\tau)\right]^{-1}\times\mathbf{E}(\omega,\tau)^T\mathbf{Y}^{(ch)}(\omega)||^2. \tag{7}$$

By solving Eq. (7), we can estimate τ. However, because $\mathbf{E}(\omega,\tau)[\mathbf{E}(\omega,\tau)^T\mathbf{E}(\omega,\tau)]^{-1}\mathbf{E}(\omega,\tau)^T$ in Eq. (7) is nonlinear with respect to τ, we cannot solve Eq. (7) analytically. We solve it by a hybrid optimization algorithm that consists of two consecutive stages: global search and local search. First, we obtain an approximate solution by global search and then obtain the optimal solution by local search. In global search, we conduct a random search (Zhigljavsky, 1991) (see Appendix A) modified from that in our previous study (Takeda et al., 2008b) for *M* (=50) times with a different initial τ. Then we obtain *M* sets of τ and o_τ $\left(=\sum_{ch=1}^{CH}\sum_{\omega=1}^{T/2}||\mathbf{Y}^{(ch)}(\omega)-\mathbf{E}(\omega,\tau)\left[\mathbf{E}(\omega,\tau)^T\mathbf{E}(\omega,\tau)\right]^{-1}\mathbf{E}(\omega,\tau)^T\mathbf{Y}^{(ch)}(\omega)||^2\right)$ and select the τ that minimizes o_τ. In local search, we conduct a grid search (see Appendix A) by setting the τ selected in global search as initial τ.

After optimization, we adjusted the averages across n of obtained τ. This adjustment is required because the averages of τ vary depending on the time points defined as the onsets of the waveforms, and the onsets are arbitrarily determined in optimization. For example, we adjusted the average of $\tau_{n,2}$ obtained from the EEGs during a NoGo task so that a peak in the estimated waveform-2 became its onsets (described in Data analysis section). Adjusted τ is referred to as $\hat{\tau}$.

Evaluation

In this step, we evaluate whether preset K is true.

As described above, once K is set, we can obtain $\hat{\tau}$ and $\hat{\mathbf{S}}^{(ch)}(\omega)$ by the steps of *Delay estimation* and *Waveform estimation*, respectively, and we can obtain the residual error between observed and reconstructed EEGs by

$$re_n^{(ch)}(t) = \mathrm{IDFT}\left[Y_n^{(ch)}(\omega) - \sum_{k=1}^{K} \exp(-i2\pi\omega\hat{\tau}_{n,k}/T)\,\hat{S}_k^{(ch)}(\omega)\right], \quad (8)$$

where IDFT[···]: inverse discrete Fourier transform of ···. We evaluate preset K by examining $re_n^{(ch)}(t)$. When preset K is smaller than true, $s_k^{(ch)}(t)$ should remain in $re_n^{(ch)}(t)$. As a result, $re_n^{(ch)}(t)$ should be a nonstationary process. In contrast, when preset K is true, $s_k^{(ch)}(t)$ should disappear from $re_n^{(ch)}(t)$. As a result, $re_n^{(ch)}(t)$ should be a stationary process. Therefore, we evaluate preset K by examining whether $re_n^{(ch)}(t)$ is a stationary process. We examine whether the distribution of $re_n^{(ch)}(t)$ differs before and after stimulus onsets. We divide all $re_n^{(ch)}(t)$ $(n=1,\cdots,N; ch=1,\cdots,CH)$ into two samples corresponding to before and after stimulus onsets, and conduct a two-tailed Two-Sample Kolmogorov–Smirnov test to test the null hypothesis that the two samples are drawn from the same distribution. The probability of $p<0.05$ is accepted as significant. If the null hypothesis is rejected, we regard preset K as wrong. If the null hypothesis comes to be accepted, we regard preset K as true.

Simulation tests

To examine the performance of the proposed method, we conducted simulation tests for *Waveform estimation*, *Delay estimation*, and *Evaluation*.

In these simulation tests, we generated simulated data $y_n^{(ch)}(t)$ as follows. We generated five waveforms, $s_1(t),\cdots s_5(t)$, by an exponential function, a cosine function, a rectangular function, a sawtooth wave, and a triangular pulse, respectively. All of the waveforms were identical regardless of channels ch. We set the variance across t of the waveforms to 1. We set the delays of $s_1(t)$ to 1 and generated the delays of the other waveforms by Gaussian random numbers [mean = 18, standard deviation (SD) = 5]. We used white noise as noise $v_n^{(ch)}(t)$. Then we generated $y_n^{(ch)}(t)$ from $s_k(t)$, τ and $v_n^{(ch)}(t)$, based on Eq. (1).

Simulation tests for Waveform estimation

To evaluate the quality of *Waveform estimation*, we scrutinized the residual errors between estimated waveforms $\hat{s}_k(t)$ and original waveforms $s_k(t)$.

First, we examined whether the residual errors fluctuated randomly around 0. We generated simulated data $y_n^{(ch)}(t)$ with the following parameters: number of waveforms $K=2$, number of channels $CH=1$, number of trials $N=100$, and signal-to-noise ratio (SNR) = 6. SNR was defined as $10\log_{10}(\mathrm{Var}[s_k(t)]/\mathrm{Var}[v_n(t)])$, where $\mathrm{Var}[s_k(t)]=1$. We repeated the estimation of $s_k(t)$ 500 times from different sets of $y_n^{(ch)}(t)$ and obtained 500 sets of residual errors. Because the averages across time of $\hat{s}_k(t)$ are inherently indefinite, we adjusted the averages across time of the residual errors to 0. We then plotted the time courses of the means and SDs of the 500 residual errors.

Second, we examined whether the magnitudes of the residual errors became smaller as the number of trials N increased. We generated $y_n^{(ch)}(t)$ with the following parameters: $K=2$, $CH=1$, $N=100,\cdots,1000$, and SNR = 6. For each N, we repeated the extraction of $s_k(t)$ 500 times from different sets of $y_n^{(ch)}(t)$ and obtained 500 sets of residual errors. The magnitudes of the residual errors were quantified by the variance across time of the residual errors:

$$\frac{1}{500\times K}\sum_{p=1}^{500}\sum_{k=1}^{K} \mathrm{Var}\left[\hat{s}_k^{(p,N)}(t) - s_k(t)\right],$$

where $\hat{s}_k^{(p,N)}(t)$ represents the p-th estimated waveform-k obtained from the simulated data consisting of N trials. The variance was fitted by function $y=a/N$ by the least squares method.

Finally, we compared error coefficients a of fitting function $y=a/N$ obtained in different situations. a represents the magnitude of the residual errors for all N, and thus a smaller value of a is better. We generated $y_n^{(ch)}(t)$ with the following parameters: $K=1,\cdots,5$, $CH=1$, $N=100,\cdots,1000$, and SNR = 6. For each K, we obtained a. Because the averaging procedure can be used when $K=1$, we also obtained a for $K=1$ using the averaging procedure. Because our previous method (Takeda et al., 2008a) can be used when $K=2$, we also obtained a for $K=2$ using that method.

Simulation tests for Delay estimation

To evaluate the quality of *Delay estimation*, we examined the normalized root mean squared errors (RMSEs) between sets of delays τ obtained in the *Delay estimation* step and true τ. RMSE was calculated by

$$\mathrm{RMSE} = \frac{1}{K}\sum_{k=1}^{K} \times\sqrt{\frac{1}{N}\sum_{n=1}^{N}\left(\left(\tau_{n,k}-\frac{1}{N}\sum_{n=1}^{N}\tau_{n,k}\right)-\left(\tau_{n,k}^{\mathrm{true}}-\frac{1}{N}\sum_{n=1}^{N}\tau_{n,k}^{\mathrm{true}}\right)\right)^2},$$

where $\tau_{n,k}$ and $\tau_{n,k}^{\mathrm{true}}$ represent delay and true delay, respectively.

First, we examined the validity of Eq. (7) and whether τ became closer to the true one as optimization proceeded. We generated simulated data $y_n^{(ch)}(t)$ with the following parameters: number of waveforms $K=3$, number of channels $CH=1$, number of trials $N=100$, and SNR = 6. From $y_n^{(ch)}(t)$ by global search, we obtained M (=50) sets of o_τ and RMSEs, and by local search, we obtained one set of those. Then we made a scatter plot of o_τ and the RMSEs.

Second, we examined the relation between estimation accuracy and SNR. We generated $y_n^{(ch)}(t)$ with the following parameters: $K=2,3$, $CH=1$, $N=100$, and SNR = -20,-15,-10,-5,0. For each K and SNR, we estimated τ and calculated RMSE. The estimation was repeated 10 times from different sets of $y_n^{(ch)}(t)$.

Finally, we examined the relation between estimation accuracy and CH. We generated $y_n^{(ch)}(t)$ with the following parameters: $K=3$, $CH=1,2,3$, $N=100$, and SNR = -5. For each CH, we estimated τ and calculated RMSE. The estimation was repeated 10 times from different sets of $y_n^{(ch)}(t)$. To examine the effect of adding meaningless channels, we also generated $y_n^{(ch)}(t)$ by

$$y_n^{(ch)}(t) = \begin{cases} \sum_{k=1}^{K} s_k\left(t-\tau_{n,k}\right) + v_n^{(ch)}(t) & ch=1 \\ v_n^{(ch)}(t) & ch>1 \end{cases},$$

and calculated RMSE in the same way. In this simulation, we refer to channels including and not including $s_k(t)$ as meaningful and meaningless channels, respectively.

Simulation tests for Evaluation

In the simulation tests for *Evaluation*, we first checked the rationale of the procedure for evaluating the number of waveforms K. We examined the time courses of the means and SDs across trials of the residual errors between the original and reconstructed simulated data. We generated simulated data $y_n^{(ch)}(t)$ with the following parameters: $K=3$, number of channels $CH=1$, number of trials $N=100$, and SNR = 6. From $y_n^{(ch)}(t)$, we obtained three sets of residual errors using a preset K of 1,2,3.

Then we examined the relation between the reliability of *Evaluation* and SNR. In the *Evaluation* step, we calculate the p-value of the null hypothesis that $re_n^{(ch)}(t)$ before and after stimulus onsets are drawn from the same distribution. Correct K is estimated if the p-value for K smaller than true is larger than 0.05 and the p-value for true K is smaller than 0.05. We obtained the probability of satisfying this condition in the following way. We generated $y_n^{(ch)}(t)$ with the following parameters: $K=3$, $CH=3$, $N=100$, and SNR = -20,-15,-10,-5,0. For each SNR, we conducted *Delay estimation* and *Waveform estimation* with preset $K=2$ (smaller than true) and $K=3$ (true), obtained two sets of $re_n^{(ch)}(t)$, and calculated the two p-values. We repeated this procedure 10 times and obtained the probability of satisfying the condition.

Applications to EEGs during Go/NoGo task

As an example, we applied the proposed method to the EEGs during a Go/NoGo task.

Experimental procedure

The experimental population was comprised of nine healthy adults (age 28.4 ± 3.7 years), all of whom gave informed consents. The local ethics committee approved the experimental procedure.

The subjects were comfortably seated on a chair in a dimly lit, electrically shielded room. About 50 cm in front of their eyes, red and green light-emitting diodes (LEDs) for imperative signals were vertically arrayed 1.5 cm apart on a black panel. The subjects were instructed to perform two tasks in the following order: a Go/NoGo task and a passive viewing task. In the Go/NoGo task, they participated in four experimental blocks, each consisting of 50 trials. They were instructed to push a button immediately after a “Go” signal (green LED) and to not push it after a “NoGo” signal (red LED). The green and red LEDs were illuminated in random order at almost equal probability. In two blocks, the subjects had to respond with their right index finger and in the other two blocks with their left index finger. In off-line analysis, the data from the blocks of the left and right fingers were mixed. In the passive viewing task, the subjects participated in two experimental blocks, each consisting of 50 trials. They were instructed to passively view the same stimulus as in the Go/NoGo task. In both tasks, each trial began with a warning signal (a beep), followed, after a variable delay of 1.8–2.2 s, by the imperative signals (duration: 500 ms). Inter-trial intervals were randomized from 3.5 to 7.5 s.

During the tasks, surface EEGs were recorded from 19-ch tin electrodes, mounted in a cap (Electro-Cap International, Inc., Eaton, Ohio, USA) based on the international 10–20 system. A tin electrode placed on AFz was used as a ground. The EEGs were amplified on a Nihon Kohden EEG-1100 with a time constant of 0.3 s. Because we expected that large EEG activity related to the task execution would not appear around the earlobes, we placed Ag/AgCl electrodes on both earlobes and recorded their potentials separately. Their averaged potentials were subtracted from the EEGs off-line. For monitoring eye movements, an electrooculogram (EOG) was recorded with a pair of Ag/AgCl electrodes placed above and below the left eye. The sampling rate of the EEGs and EOGs was 1000 Hz.

Data analysis

In the off-line analysis, we resampled the EEGs at a rate of 100 Hz. They were filtered with a bandpass of 2–40 Hz using two kinds of finite impulse response (FIR) filters: a high-pass filter of 2 Hz (300-point, -26 dB at 1 Hz) and a low-pass filter of 40 Hz (15-point, -45 dB at 50 Hz). Then the filtered EEGs were segmented into 2 s epochs from -500 to 1500 ms after stimulus onsets.

If waveforms common across trials exist in EEGs, their mean and SD across trials should change with time. The time courses of the means and SDs of a subject's EEGs during the Go/NoGo task at Fz, C3, C4, Cz, and Pz clearly showed transient changes, indicating the existence of such waveforms in these EEGs. Therefore, we applied the proposed method to them.

The reaction times (RTs) of the Go trials were defined as the intervals between the stimulus and the button-push signal (response) onsets. We excluded the Go trials with an RT either shorter than 100 ms or longer than 400 ms, and the NoGo trials with any response. An artifact criterion of ±50 μV was used for the EEGs and EOGs to reject trials with excess ocular artifacts or measurement noise. We obtained 96 Go trials and 100 NoGo trials. The RTs were 275.63 ± 46.24 (mean ± SD) ms.

In the *Delay estimation* step, we estimated the delays of the EEG waveforms common across trials using priori knowledge about the delays. In the Go/NoGo task, the approximate delays of two waveforms can be given from the stimulus and the response onsets; using the delays simplifies the optimization problem [Eq. (7)]. We assumed that the delays of waveform-1s slightly fluctuate after the stimulus onsets and the delays of waveform-2s in the Go trials slightly fluctuate around the response onsets. Therefore, based on reports that examined the variable latencies of visual evoked potentials (Mihaylova et al., 1999; Vassilev et al., 2002; Vaughan et al., 1966), we searched for the delays of waveform-1s from 0 to 50 ms after the stimulus onsets and the delays of waveform-2s in the Go trials from -25 to 25 ms after the response onsets. We searched for the delays of the other waveforms setting the initial delays to Gaussian random numbers [mean = 180 (ms), SD = 50 (ms)]. We set the delay ranges at a width of 500 ms because the EEGs' SDs, which are indications of the variable delays (Takeda et al., 2008b), were clearly greater than the pre-stimulus level for about 500 ms after the stimulus onset. After the optimization of Eq. (7), we adjusted the delays of the estimated waveforms. The delays of waveform-1s were adjusted so that the minimum values of the estimated delays became 0 ms. The delays of waveform-2s in the Go trials were adjusted so that the average of the estimated delays was identical with that of the RTs. The delays of the other waveforms were adjusted so that the estimated delays represented the latencies of the maximum positive peak in each of the estimated waveforms at Cz. In the *Waveform estimation* step, we estimated the waveforms using the estimated delays. For comparison with the estimated waveform-1s, we obtained stimulus-triggered average EEGs by averaging the EEGs triggered on the stimulus onsets. For comparison with the estimated waveform-2s in the Go trials, we also obtained response-triggered average EEGs by averaging the EEGs during the Go trials triggered on the response onsets. In the *Evaluation* step, we evaluated whether the preset number of waveforms was true. We compared the distributions of the residual errors at Fz, C3, C4, Cz, and Pz from -0.5 to 0 s with those from 0 to 0.7 s after the stimulus onsets.

After the estimation, using the estimated delays, we estimated the waveforms from the 19-channel EEGs by the *Waveform estimation* procedure and obtained the scalp distributions of the variance across time of the estimated waveforms. Finally, because the estimated waveforms seemed to have large oscillatory components, we calculated the amplitude spectra by taking the discrete Fourier transform of $h(t)\hat{s}_k^{(ch)}(t)$, where $h(t)$ was the Hanning window. We calculated the amplitude spectra at Fz, Cz, and Pz and averaged them across the channels. For comparison, we also calculated the amplitude spectra of the stimulus- and response-triggered average EEGs in the same way.

Results

Simulation tests

Figs. 2A–D shows original waveforms $s_k(t)$ $(k=1,2,3)$ and noise $v_n^{(ch)}(t)$. Fig. 2E shows simulated data $y_n^{(ch)}(t)$ generated with the

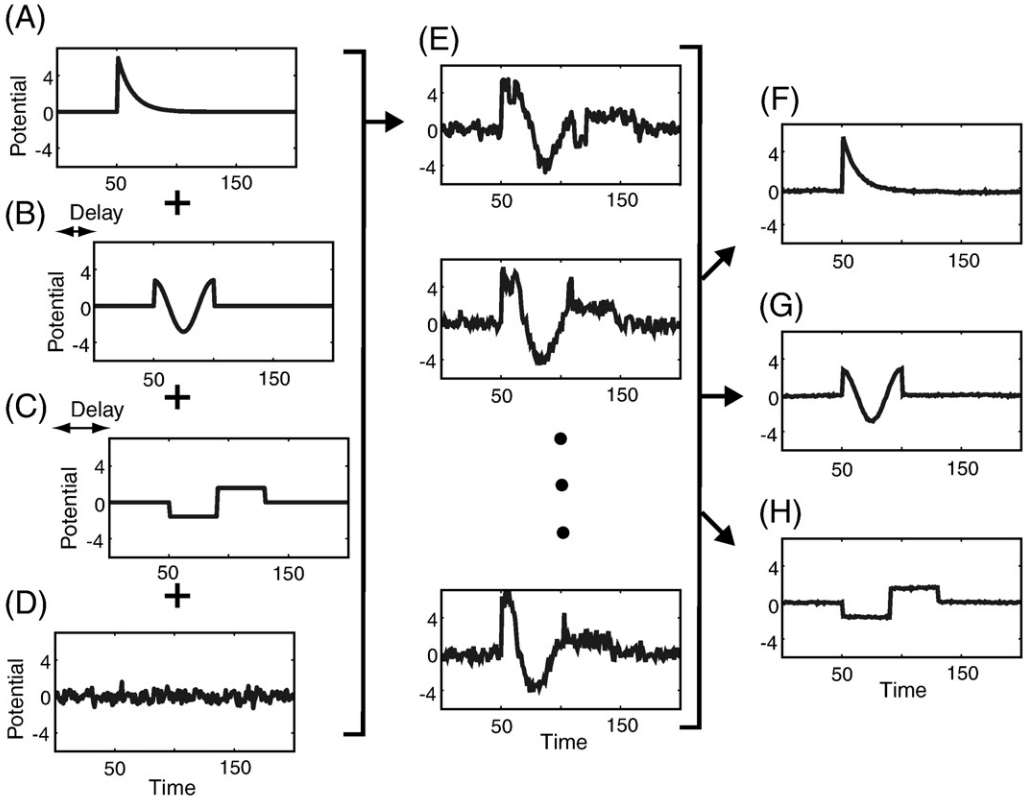

Fig. 2. Simulation tests for overall procedure. (A–D) Original waveforms $s_k(t)$ and noise $v_n^{(ch)}(t)$. (A) $s_1(t)$. (B) $s_2(t)$. (C) $s_3(t)$. (D) $v_n^{(ch)}(t)$. (E) Simulated data $y_n^{(ch)}(t)$ generated from $s_1(t)$, $s_2(t)$, $s_3(t)$, and $v_n^{(ch)}(t)$. (F–H) Estimated waveforms $\hat{s}_k(t)$. (F) $\hat{s}_1(t)$. (G) $\hat{s}_2(t)$. (H) $\hat{s}_3(t)$.

following parameters: number of waveforms $K=3$, number of channels $CH=1$, number of trials $N=100$, and SNR$=6$. Before proceeding to the simulation tests for the individual steps, we examined whether the overall procedure (Fig. 1) worked well. From the simulated data (Fig. 2E), we estimated K, the delays of waveforms τ, and the $s_k(t)$ (Figs. 2F–H). Estimated K is correctly 3. Estimated $s_k(t)$ are highly correlated with the original ones; all of the correlation coefficients between the estimated and original $s_k(t)$ are higher than 0.99 (Figs. 2F–H). The RSMEs between the estimated and original τ are 0, indicating that the estimation is completely accurate. These results indicate that the proposed method, as a whole, works well for the simulated data.

Simulation tests for Waveform estimation

Fig. 3 shows the results of the simulation tests for *Waveform estimation*. Figs. 3A and B shows the time courses of the means and SDs of the residual errors between the estimated and original waveforms. These time courses are nearly constant (Figs. 3A and B), indicating that

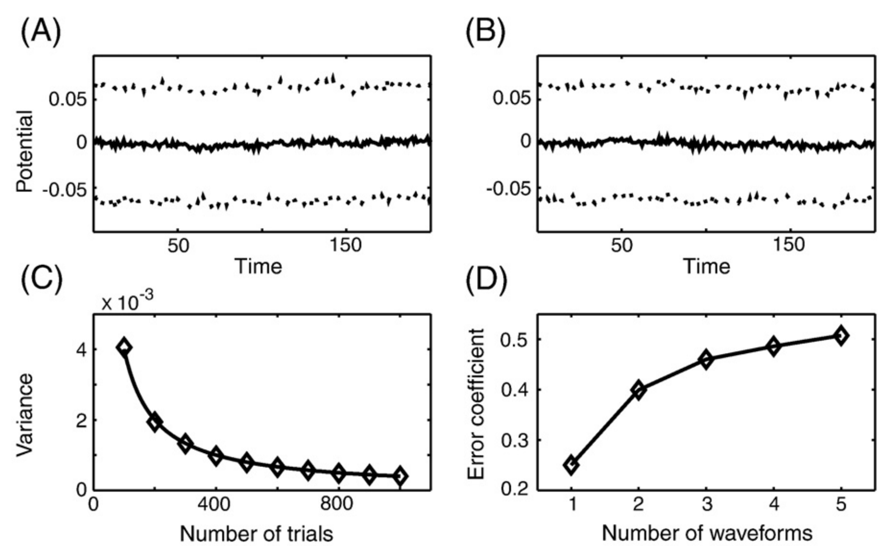

Fig. 3. Simulation tests for *Waveform estimation*. (A, B) Means (solid lines) and means ± SDs (dotted lines) of residual errors between estimated and original waveforms across 500 repeated simulations. (A) Result for estimated waveform-1 $\hat{s}_1(t)$. (B) Result for estimated waveform-2 $\hat{s}_2(t)$. (C) Variance of residual errors as function of number of trials N (diamonds). Solid lines represent fitting curves in form of $y=a/N$. (D) Error coefficient a of fitting function $y=a/N$ for each number of waveforms K.

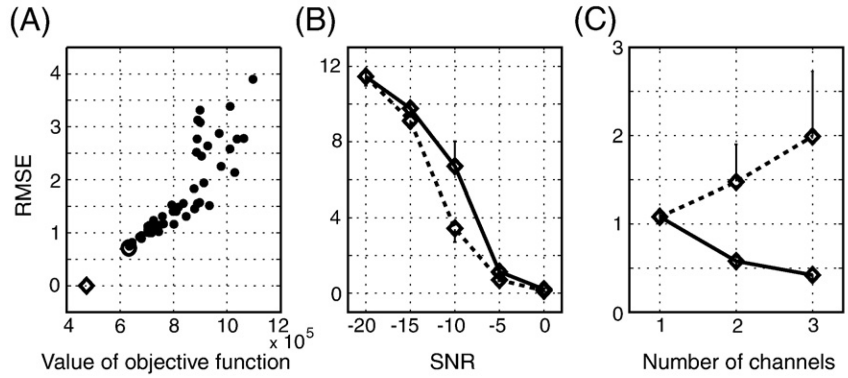

Fig. 4. Simulation tests for *Delay estimation*. (A) Scatter plots of values of objective function o_τ and RMSEs between estimated and original delays τ. Open circle indicates selected τ in global search. Filled dots indicate non-selected τ in global search. Diamond indicates converged τ in following local search. (B) RMSEs between estimated and original τ for each SNR. Solid line represents results for number of waveforms $K=3$. Dotted line represents results for $K=2$. (C) RMSEs between estimated and original τ for each number of channels *CH*. Solid line represents results for adding meaningful channels. Dotted line represents results for adding meaningless channels. In (B) and (C), diamonds and error bars respectively represent means and SDs of RMSEs.

the residual errors have no temporal modulation patterns and fluctuate randomly. Fig. 3C shows how the variance of the residual errors changes as the number of trials N increases. The variance is inversely proportional to N (Fig. 3C), indicating that the residual errors become smaller as the number of trials increases. Fig. 3D shows how error coefficients a of fitting function $y=a/N$ changes as the number of waveforms K increases. a becomes larger as K increases, indicating that the accuracy of the estimated waveforms becomes lower as the number of waveforms increases. When $K=1$, the a of the averaging procedure is 0.25, which is the same as that of the *Waveform estimation* procedure. This indicates that the accuracy of the *Waveform estimation* procedure is identical as that of the averaging procedure. When $K=2$, the a of our previous method (Takeda et al., 2008a) is 1.91, which is larger than that of the *Waveform estimation* procedure. This indicates that the accuracy of the *Waveform estimation* procedure is higher than that of our previous method (Takeda et al., 2008a).

Simulation tests for Delay estimation

Fig. 4 shows the results of the simulation tests for *Delay estimation*. Fig. 4A is the scatter plot of RMSEs between the estimated and original delays τ and the values of objective function o_τ. RMSE becomes smaller as o_τ becomes smaller, suggesting the validity of Eq. (7). RMSE of selected τ in global search (open circle) is smallest among those of non-selected τ (filled dots), indicating the validity of global search. RMSE of $\hat{\tau}$ obtained by local search (diamond) is smaller than that of the selected τ in global search (open circle), indicating the validity and necessity of local search. Fig. 4B shows the relations between RMSEs and SNR. RMSEs become smaller as SNR becomes higher, indicating that the estimation accuracy becomes higher as SNR becomes higher. For SNRs of -15,-10,-5,0, RMSEs for the number of waveforms $K=2$ (dotted line) are significantly smaller than those for $K=3$ (solid line) ($p<0.05$, two-tailed Mann–Whitney test), indicating that the estimation accuracy for $K=2$ is higher than that for $K=3$. Fig. 4C shows the relations between RMSEs and the number of channels *CH*. While RMSEs obtained by adding meaningful channels (solid line) become smaller as *CH* increases, those by adding meaningless channels (dotted line) become larger. This indicates that adding meaningful channels increases estimation accuracy but not adding meaningless channels.

Simulation tests for Evaluation

Fig. 5 shows the results of the simulation tests for *Evaluation*. Fig. 5A shows the time course of the means and SDs of the residual errors between the original and reconstructed simulated data. When the preset number of waveforms K is smaller than true ($K=1,2$), the residual errors are nonstationary; the time courses of the means and/

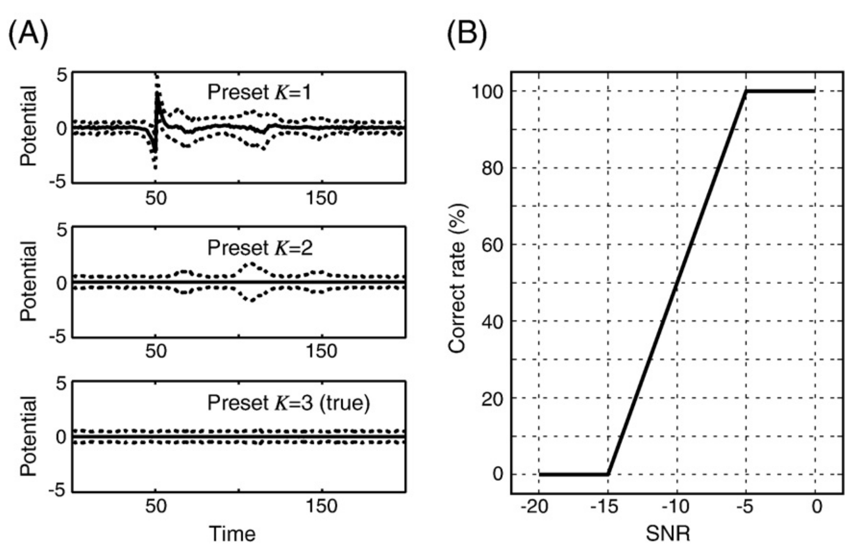

Fig. 5. Simulation tests for *Evaluation*. (A) Means (solid lines) and means ± SDs (dotted lines) across trials of residual errors between original and reconstructed simulated data. (B) Correct rate (%) of estimating true number of waveforms K for each SNR.

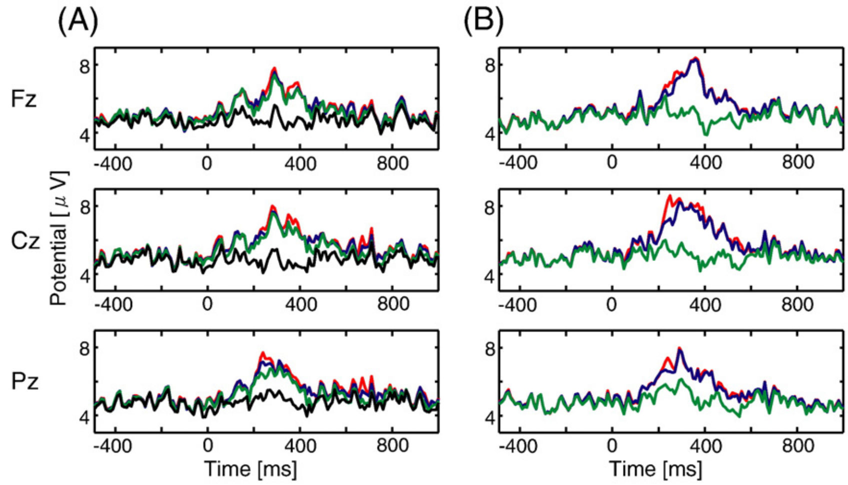

Fig. 6. SDs across trials of residual errors obtained from EEGs at Fz, Cz, and Pz. (A) Go trials. (B) NoGo trials. Red lines represent SDs across trials of EEGs during Go/NoGo task. Blue, green, and black lines respectively represent SDs across trials of residual errors for preset K of 1, 2, and 3. Time 0 corresponds to stimulus onsets.

or SDs of the residual errors are not constant. In contrast, when preset K is true ($K = 3$), the residual errors are stationary; the time courses of the means and SDs of the residual errors are constant. These results indicate the rationale of the *Evaluation* procedure. Fig. 5B shows the relations between the correct rates (%) of estimating true K and SNR. The correct rates become higher as SNR becomes higher, indicating that the reliability of *Evaluation* becomes higher as SNR becomes higher.

Application to EEGs during Go trials

Figs. 6A, 7, 8, and 9 show the results of applying the proposed method to the EEGs during the Go trials. Fig. 6A shows the SDs across the trials of the residual errors between the original and reconstructed EEGs. When 3 is the preset number of waveforms, the time courses of the means and the SDs of the residual errors become almost constant and the number of waveforms is estimated to be 3. Figs. 7, 8, and 9A show the estimated waveforms at Fz, Cz, and Pz. The correlation coefficient between the estimated waveform-1 at Cz and the stimulus-triggered average EEG at Cz is 0.67, indicating that both waveforms are similar (Fig. 7A, middle). Waveform-1s exhibit P300 as well as the stimulus-triggered average EEGs (Fig. 7A). Waveform-1s have large oscillatory components around 700 ms after the stimulus onsets (Fig. 7A). The correlation coefficient between the estimated waveform-2 at Cz and the response-triggered average EEG at Cz is 0.54, indicating that both waveforms are similar (Fig. 8A, middle). Waveform-2s have large oscillatory components around 400 ms after the response onsets. Figs. 7, 8, and 9B show the histograms of the

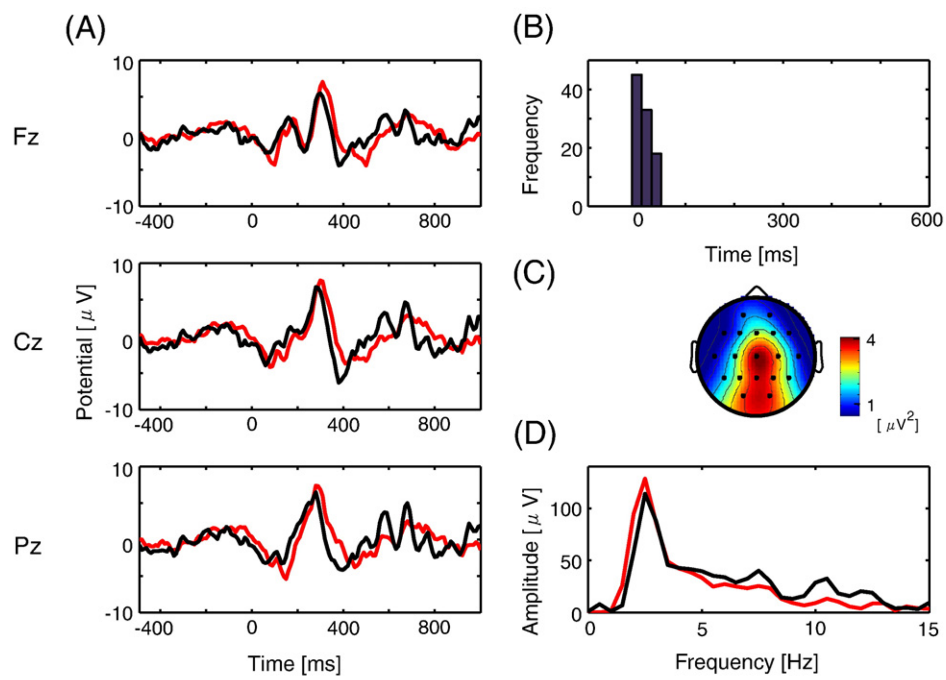

Fig. 7. Estimated waveform-1s from EEGs during Go trials. (A) Estimated waveform-1s at Fz, Cz, and Pz (black lines). Red lines represent stimulus-triggered average EEGs at Fz, Cz, and Pz. Time 0 corresponds to stimulus onset. (B) Histograms of delays of estimated waveform-1s. Time 0 corresponds to stimulus onset. (C) Scalp distributions of variance across time of estimated waveform-1s. (D) Average amplitude spectra of estimated waveform-1s at Fz, Cz, and Pz (black line). Red line represents average amplitude spectra of stimulus-triggered average EEGs at Fz, Cz, and Pz.

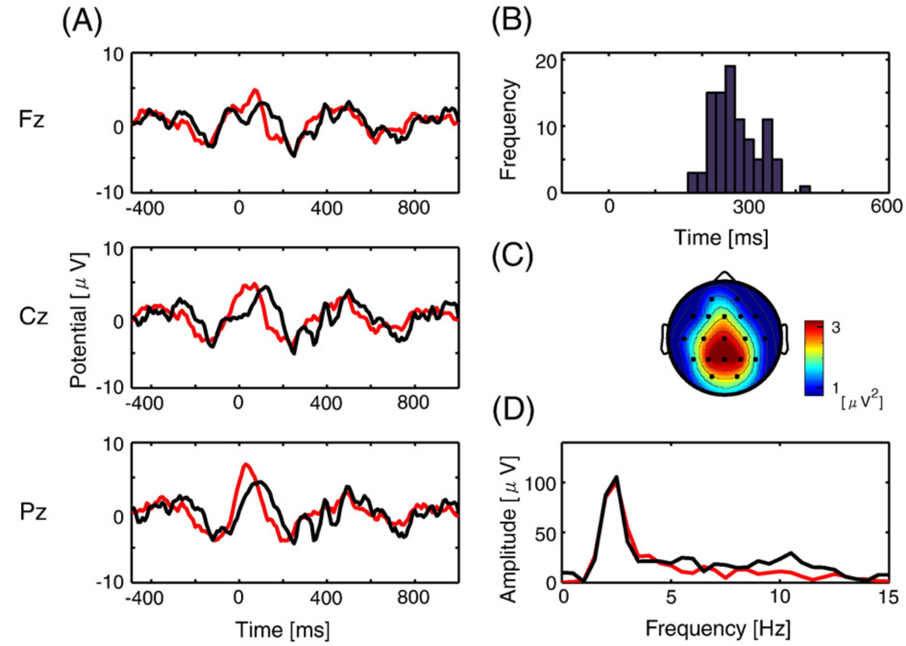

Fig. 8. Estimated waveform-2s from EEGs during Go trials. (A) Estimated waveform-2s at Fz, Cz, and Pz (black lines). Red lines represent response-triggered average EEGs at Fz, Cz, and Pz. Time 0 corresponds to button-push signal onset. (B) Histograms of delays of estimated waveform-2s. Time 0 corresponds to stimulus onset. (C) Scalp distributions of variance across time of estimated waveform-2s. (D) Average amplitude spectra of estimated waveform-2s at Fz, Cz, and Pz (black line). Red line represents average amplitude spectra of response-triggered average EEGs at Fz, Cz, and Pz.

delays of the estimated waveforms. The estimated delays are 18.54 ± 14.87 ms for waveform-1s, 276.25 ± 47.95 ms for waveform-2s, and 329.48 ± 125.58 ms for waveform-3s. Figs. 7, 8, and 9C show the scalp distributions of the variance across time of the estimated waveforms. All have large variance around Cz. Waveform-1s also have large variance around O1 and O2. Figs. 7, 8, and 9D show the average amplitude spectra of the estimated waveforms at Fz, Cz, and Pz. All have large amplitude spectra around 2–3 Hz, and waveform-3s also have large amplitude spectra around 4 Hz. Wave form-1s and waveform-2s have larger amplitude spectra around 10 Hz than the stimulus- and response-triggered average EEGs, respectively.

Application to EEGs during NoGo trials

Figs. 6B, 10, and 11 show the results of applying the proposed method to the EEGs during the NoGo trials. Fig. 6B shows the SDs across the trials of the residual errors between the original and

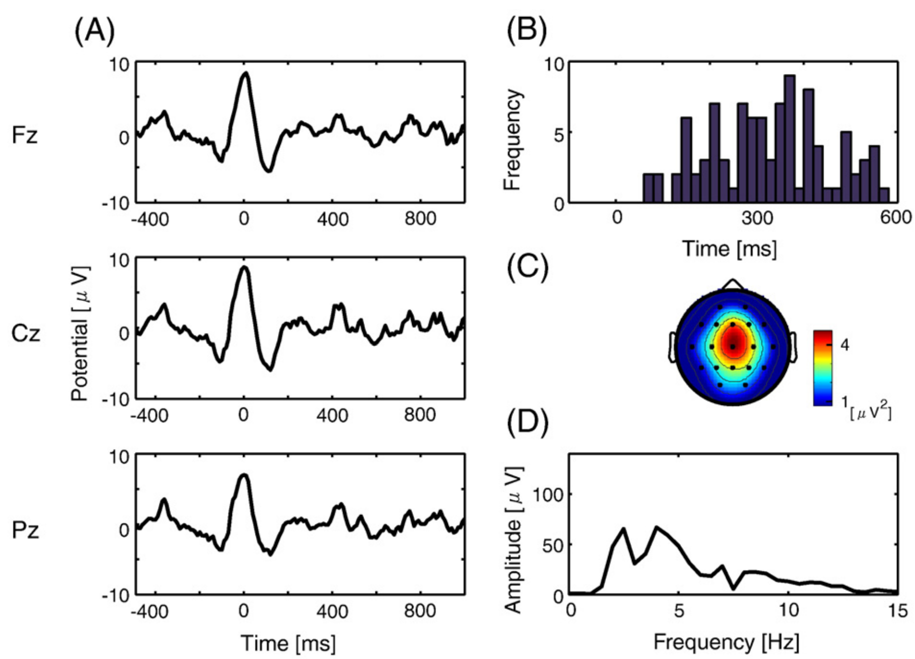

Fig. 9. Estimated waveform-3s from EEGs during Go trials. (A) Estimated waveform-3s at Fz, Cz, and Pz. Horizontal axes represent relative time to defined onsets of estimated waveform-3s. (B) Histograms of delays of estimated waveform-3s. Time 0 corresponds to stimulus onset. (C) Scalp distributions of variance across time of estimated waveform-3s. (D) Average amplitude spectra of estimated waveform-3s at Fz, Cz, and Pz.

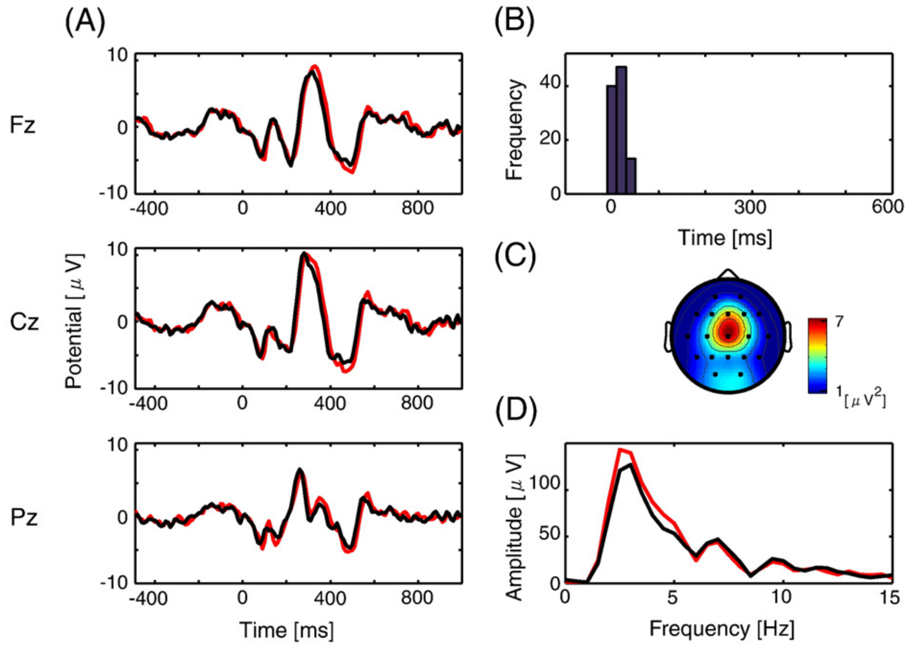

Fig. 10. Estimated waveform-1s from EEGs during NoGo trials. (A) Estimated waveform-1s at Fz, Cz, and Pz (black lines). Red lines represent stimulus-triggered average EEGs at Fz, Cz, and Pz. Time 0 corresponds to stimulus onset. (B) Histograms of delays of estimated waveform-1s. Time 0 corresponds to stimulus onset. (C) Scalp distributions of variance across time of estimated waveform-1s. (D) Average amplitude spectra of estimated waveform-1s at Fz, Cz, and Pz (black line). Red line represents average amplitude spectra of stimulus-triggered average EEGs at Fz, Cz, and Pz.

reconstructed EEGs. When 2 is the preset number of waveforms, the time courses of the means and the SDs of the residual errors become almost constant and the number of waveforms is estimated to be 2. Figs. 10 and 11A show the estimated waveforms at Fz, Cz, and Pz. The correlation coefficient between the estimated waveform-1 at Cz and the stimulus-triggered average EEG at Cz is 0.95, indicating that both waveforms are similar (Fig. 10A, middle). Waveform-1s exhibit N200 and P300 as well as the stimulus-triggered average EEGs (Fig. 10A). Figs. 10 and 11B show the histograms of the delays of the estimated waveforms. The estimated delays are 18.10 ± 12.53 ms for waveform-1s, and 336.30 ± 109.61 ms for waveform-2s. Figs. 10 and 11C show the scalp distributions of the variance across time of the estimated waveforms. All have large variance around Cz. Waveform-1s also have large variance around O1 and O2. Figs. 10 and 11D show the average amplitude spectra of the estimated waveforms at Fz, Cz, and Pz. All have large amplitude spectra around 2–3 Hz, and waveform-2s also have large amplitude spectra around 5 Hz.

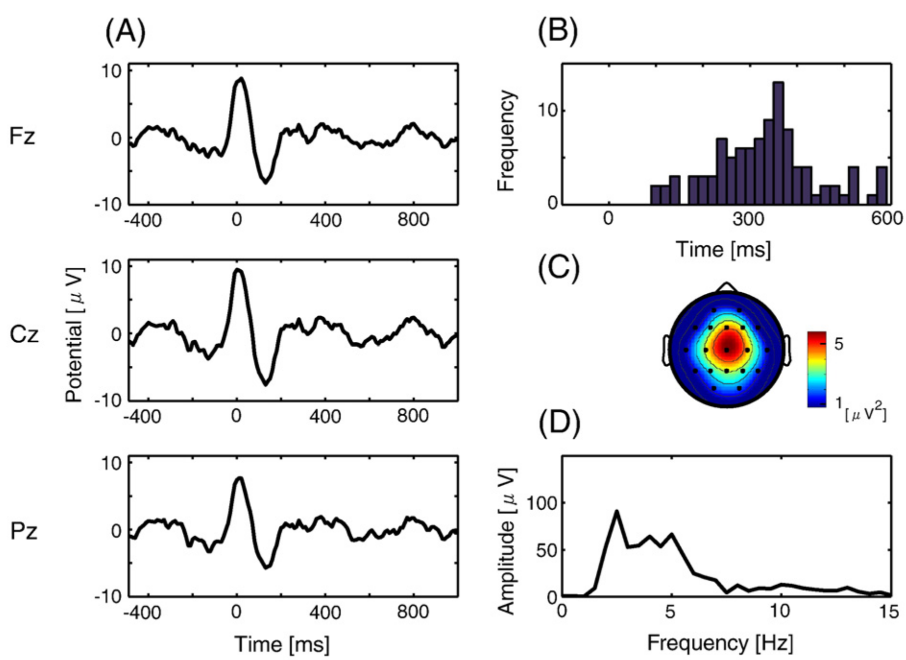

Fig. 11. Estimated waveform-2s from EEGs during NoGo trials. (A) Estimated waveform-2s at Fz, Cz, and Pz. Horizontal axes represent relative time to defined onsets of estimated waveform-2s. (B) Histograms of delays of estimated waveform-2s. Time 0 corresponds to stimulus onset. (C) Scalp distributions of variance across time of estimated waveform-2s. (D) Average amplitude spectra of estimated waveform-2s at Fz, Cz, and Pz.

Discussion

In this study, we proposed a generalized method to estimate EEG waveforms common across trials. From single/multi-channel EEGs, the method estimates the number of waveforms common across trials, the delays of waveforms, and all of the waveforms. The performance of the algorithm was verified by a number of simulation tests. We also applied this method to EEGs during a Go/NoGo task.

The purpose of the proposed method, estimating all EEG waveforms common across trials, is much more demanding than the tasks of our previous methods (Takeda et al., 2008a; Takeda et al., 2008b) and the other methods for estimating a waveform whose delays are variable and unknown (Biggins et al., 1997; Jaśkowski and Verleger, 1999, 2000; McGillem et al., 1985; Möcks et al., 1988; Pham et al., 1987; Puce et al., 1994a,b; Woody, 1967). We achieved such a demanding goal with a step-by-step approach. We divided our purpose into three easier subproblems (estimate waveforms, estimate their delays, and estimate their number) and solved the subproblems step-by-step, as shown in Fig. 1. This strategy is an essential point in the versatility of the proposed method.

Another method for separating EEGs is spatial decomposition by independent component analysis (ICA) (Jung et al., 2001; Makeig et al., 2004). ICA is a computational method for decomposing multichannel data into mutually independent components with different scalp distributions. Therefore, to separate waveforms by ICA, the EEGs need to satisfy the following three conditions: (1) the number of channels is larger than that of the waveforms, (2) the variability of the delays of waveforms is adequately large, and (3) the waveforms have different scalp distributions. Condition 1 is needed because ICA cannot distinguish a number of signals larger than the channels. Condition 2 is needed because ICA cannot distinguish correlated signals. When the delays of waveforms are within a small range, a waveform tends to overlap on certain phases of the other waveforms, and their time series tend to be correlated with each other. In fact, in our simulation test, ICA did not separate waveforms when the variability of the delays was small (data not shown). Condition 3 is needed because ICA cannot distinguish signals attributable to identical sources. In fact, in our simulation test, ICA did not separate waveforms when the source of the waveforms was the same (data not shown). We decomposed the EEGs during the Go/NoGo trials into independent components by ICA, and applied the proposed method to the components. As a result, two or more waveforms were estimated from some of the components (data not shown), indicating that the EEGs during the Go/NoGo trials did not satisfy the three conditions. In contrast to ICA, the proposed method does not need these three conditions. Therefore, from the viewpoint of estimating waveforms common across trials, we consider our method better than ICA.

The proposed method consists of three steps: *Delay estimation*, *Waveform estimation*, and *Evaluation*. Below, we discuss the three steps individually.

Waveform estimation

In the *Waveform estimation* step, we estimate waveforms common across trials when the number and the delays of waveforms are given. The validity of the procedure is verified by the simulation results (Fig. 3).

When the number of waveforms is 2, the purpose of *Waveform estimation* is almost the same as that of our previous method (Takeda et al., 2008a). However, their performances are different. A comparison of error coefficients a of *Waveform estimation* and our previous method (Takeda et al., 2008a) indicates the superiority of the *Waveform estimation* procedure. This is due to the differences between their procedures. In our previous method (Takeda et al., 2008a), waveforms were estimated by algebraically solving equation $y_n^{(ch)}(t) = s_1^{(ch)}(t) + s_2^{(ch)}(t\text{-}\tau_n) + v_n^{(ch)}(t)$ with some averaging procedures. As a result, our previous method has a limitation: slow waves (~1 Hz) in noise are amplified by the estimation. In the *Waveform estimation* procedure, waveforms are estimated by the least squares method, which somehow eliminates the limitation. Therefore, it appears best to adopt the *Waveform estimation* procedure rather than our previous method (Takeda et al., 2008a), even when the number of waveforms is known to be 2.

Delay estimation

In the *Delay estimation* step, we estimate the delays of waveforms common across trials by solving the optimization problem of Eq. (7). The validity of Eq. (7) and the procedure for solving it are verified by the simulation results (Fig. 4A).

The simulation results in Fig. 4B show that estimation accuracy is low when SNR is low. This is because, when SNR is low, wrong delays tend to minimize the value of objective function o_τ more than true delays. Consequently, the validity of Eq. (7) becomes low when SNR is low. On the other hand, the simulation results in Fig. 4C indicate that, when noise is independent across channels, estimation accuracy increases as the number of meaningful channels increases. This suggests a solution for improving estimation accuracy when SNR is low: adding meaningful channels.

The simulation results in Fig. 4B also show that estimation accuracy becomes lower when the number of waveforms increases. This is due to the increased difficulty of optimization. As the number of waveforms increases, the number of delays to be searched for increases and the difficulty of optimization increases. Therefore, when there seems to be many waveforms whose delays are unknown, we need to spend much time for optimization or to find better optimization algorithms.

Evaluation

In the *Evaluation* step, we evaluate whether the preset number of waveforms common across trials is true by examining the residual errors between original and reconstructed EEGs. The rationale of the procedure for *Evaluation* is verified by the simulation results (Fig. 5A).

To select a criterion for evaluating the preset number of waveforms, by using simulated data (not shown), we tested various criteria, such as Akaike's information criterion (AIC) (Akaike, 1974) and the cross-validation method. Among the criteria we tested, the procedure used in this study is the best from the viewpoint of providing stable and reasonable performance (Fig. 5B).

The simulation results in Fig. 5B show that the reliability of *Evaluation* is low when SNR is low. This is because, as SNR becomes lower, residual errors become more noisy, and testing whether the distributions of residual errors before and after stimulus onsets are the same becomes more difficult. Therefore, to increase the reliability of *Evaluation*, we need to increase SNR.

It is possible that the numbers of waveforms are different across channels. For example, EEGs at distant electrodes may have a different number of waveforms, e.g., 1 waveform for electrode-1 and 2 waveforms for electrode-2. In such cases, the proposed method estimates the maximum number of waveforms, and some waveforms estimated from EEGs that have the smaller number of waveforms become flat. In the above example, the estimated number of waveforms should be 2, and one of the waveforms estimated from EEGs at electrode-1 should be flat. Therefore, we can know the effective number of waveforms for each channel by examining estimated waveforms.

Some extended usages

We have described a basic usage of our method to estimate EEG waveforms common across trials. In practice, we can use this method in a variety of ways depending on our needs and situations. For example, only the *Waveform estimation* step is needed when we estimate the approximate waveforms of stimulus- and response-locked components (Braun et al., 2002; Endo et al., 1999; Goodin et al., 1986; Jung et al., 2001; Makeig et al., 2004) from EEGs during stimulus–response tasks. Further, we can easily extend the method. We describe some extended usages of the methods below.

Using a priori knowledge about importance of channels and frequencies

Sometimes, we have a priori knowledge about the importance of channels and/or frequencies. For example, EEGs at frontal channels are sometimes contaminated with EOG and have low SNR. Further, EEGs at high frequencies (>50 Hz) are sometimes contaminated with electromyographic activity. In such cases, using these channels and frequencies as well as others may decrease the accuracy of the estimation, as shown in Fig. 4C. In the *Delay estimation* step, we can use the knowledge about the importance of channels and frequencies by replacing Eq. (7) with

$$\hat{\tau} = \underset{\tau}{\operatorname{argmin}} \sum_{ch=1}^{CH} W_{ch}(ch) \sum_{\omega=1}^{T/2} W_{\omega}(\omega) \,||\, \mathbf{Y}^{(ch)}(\omega) - \mathbf{E}(\omega,\tau) \times \left[\mathbf{E}(\omega,\tau)^{\mathrm{T}}\mathbf{E}(\omega,\tau)\right]^{-1} \mathbf{E}(\omega,\tau)^{\mathrm{T}}\mathbf{Y}^{(ch)}(\omega) \,||\,^{2}, \tag{9}$$

where $W_{ch}(ch)$: a weight function of ch, and $W_{\omega}(\omega)$: a weight function of ω.

Using a priori knowledge about delays of waveforms

Sometimes we have a priori knowledge about the delays of EEG waveforms common across trials. For example, in stimulus–response tasks, the approximate delays of two waveforms can be given from stimulus and response onsets. In such cases, using the given delays simplifies the optimization problem [Eq. (7)] and may increase estimation accuracy. In the *Delay estimation* step, we can use the knowledge about the delays by restricting the delays' search space to the neighborhood of the given delays.

Using a priori knowledge about waveforms

Sometimes we have a priori knowledge about EEG waveforms common across trials. For example, an approximate waveform can be given by averaging EEGs triggered on stimulus onsets. In such cases, using known waveforms simplifies the optimization problem [Eq. (7)] and may increase the estimation accuracy. In the *Delay estimation* step, we can use the knowledge about waveforms by replacing Eq. (7) with

$$\hat{\tau} = \underset{\tau}{\operatorname{argmin}} \sum_{ch=1}^{CH} \sum_{\omega=1}^{T/2} ||\, \mathbf{Y}^{(ch)}(\omega) - \mathbf{E}_1(\omega,\tau_1)\mathbf{S}_1^{(ch)}(\omega) - \mathbf{E}_2(\omega,\tau_2) \times \left[\mathbf{E}_2(\omega,\tau_2)^{\mathrm{T}}\mathbf{E}_2(\omega,\tau_2)\right]^{-1} \mathbf{E}_2(\omega,\tau_2)^{\mathrm{T}}\left(\mathbf{Y}^{(ch)}(\omega) - \mathbf{E}_1(\omega,\tau_1)\mathbf{S}_1^{(ch)}(\omega)\right) ||^{2}, \tag{10}$$

where $\mathbf{S}_1^{(ch)}(\omega)$: a L-by-1 matrix generated from known L waveforms, $\mathbf{E}_1(\omega,\tau_1)$: a N-by-L matrix generated from τ_1 [$=\tau_{n,k}(n=1,\cdots,N;k=1,\cdots,L)$], and $\mathbf{E}_2(\omega,\tau_2)$: a N-by-(K-L) matrix generated from τ_2 [$=\tau_{n,k}(n=1,\cdots,N;k=L+1,\cdots,K)$].

Using waveform correlation across channels

In the case of low spatial resolution data, such as EEGs, waveforms are correlated across channels. For example, waveforms at O1 may resemble those at O2 because the two electrodes are close to each other. In such cases, using the waveform correlation may increase the estimation accuracy. There are two ways to use the waveform correlation: (1) by using spatial decomposition techniques before applying our method, and (2) by assuming a model that incorporates the waveform correlation. In the first case, we first decompose EEGs by spatial decomposition techniques, such as ICA or principal component analysis (PCA). Then, we apply the proposed method to the decomposed components. Because the decomposition techniques separate signals from noises, the estimation accuracy increases. In the second case, we assume, for example, a model in which temporal waveforms are the same but their amplitudes are different across channels. In this model, an EEG can be expressed by

$$y_n^{(ch)}(t) = \sum_{k=1}^{K} a_k(ch)s_k\left(t-\tau_{n,k}\right) + v_n^{(ch)}(t), \tag{11}$$

where $y_n^{(ch)}(t)$: observed EEG epoch of channel ch in trial n, $a_k(ch)$: amplitude of k-th waveform of channel ch, $s_k(t)$: k-th waveform, $\tau_{n,k}$: delay of $s_k(t)$ in trial n, $v_n^{(ch)}(t)$: noise of channel ch in trial n, and K: number of waveforms.

The unknown parameters $a_k(ch)$, $s_k(t)$, $\tau_{n,k}$, and K can be estimated in an iterative way. When Eq. (11) is valid, its estimation accuracy would be higher than that of Eq. (1) because Eq. (11) has fewer parameters than Eq. (1). In fact, in our preliminary simulation test, the estimation accuracy of Eq. (11) was higher (data not shown).

Target data

We focused on EEGs, but the proposed method can also be applied to other kinds of brain imaging data, such as magnetoencephalography (MEG) data. Also, the method can be applied to preprocessed EEG/MEG data. For example, the method can be applied to time-frequency data, such as a scalogram obtained by taking a wavelet transform of EEG/MEG. In this case, $y_n^{(ch)}(t)$ in Eq. (1) is regarded as the value of time-frequency data at time t and frequency ch.

Limitation

Although the proposed method seems generally useful for wide EEG analyses, it also has an inherent limitation: the validity of the assumption [Eq. (1)]. The proposed method assumes that noise is a stationary process, and in the *Evaluation* step, nonstationary residual errors are due to the remaining waveforms common across trials. However, it is possible that the nonstationary residual errors are due to other factors. Nonstationary background noise or the variability of waveforms (Mihaylova et al., 1999; Vassilev et al., 2002; Vaughan et al., 1966) may be responsible for the nonstationary residual errors. In such cases, the proposed method may extract nonexistent false waveforms. To prevent this, before applying the proposed method, we need to examine whether the nonstationary residual errors are actually due to waveforms common across trials.

Applications to EEGs during Go/NoGo task

Before applying the proposed method to the EEGs during the Go/NoGo task, we examined whether nonstationary EEGs are due to other factors than waveforms common across trials. We focused on the SDs of the EEGs across the trials and examined whether the increased SDs after the stimulus onsets (Fig. 6, red lines) are due to other factors than the variable delays of waveforms common across trials.

We examined whether the variability in the amplitudes of waveforms was responsible for the increased SDs. From the EEGs during the Go trials, we estimated stimulus- and response-locked waveforms by the *Waveform estimation* procedure using the RTs, estimated the trial-to-trial variability of the amplitudes of the estimated waveforms by the least squares method, and obtained residual errors. As a result, increases in the residual errors' SDs still occurred (data not shown). From the EEGs during the NoGo trials, we estimated stimulus-locked waveforms by the stimulus-triggered averaging procedure, estimated the trial-to-trial variability of the amplitudes of the estimated waveforms by the least squares method, and obtained the residual errors. As a result, increases in the residual errors' SDs still occurred (data not shown). Therefore, we concluded that the variability of the amplitudes of the waveforms was not fully responsible for the increased SDs during the Go/NoGo task. Furthermore, we examined whether the stimulus increased the amplitude of the background noise and whether the increased background noise was responsible for the increased SDs. We examined the SDs of the EEGs during the passive viewing task. Since the SDs did not show such drastic increases as the EEGs during the Go/NoGo task (see Takeda et al., 2008b), we concluded that the increased background noise by the stimulus was not fully responsible for the increased SDs during the Go/NoGo task. Based on these preliminary examinations, we assumed the validity of the assumption [Eq. (1)] for the EEGs during the Go/NoGo tasks and thus applied the proposed method to the EEGs.

From the EEGs during the Go/NoGo tasks, for the first time we estimated the numbers of waveforms common across trials, their delays, and all of the waveforms. As the preset number of waveforms increases, the time courses of the SDs of the residual errors become more constant (Fig. 6). This suggests that the estimated waveforms and their delays are responsible for the increased SDs. The estimated waveforms are discussed below.

Waveforms time-locked to stimulus onsets

Waveform-1s in the Go and NoGo trials are stimulus-locked. Therefore, waveform-1s are considered to reflect stimulus-related brain processes, such as perception of the visual stimuli. This is confirmed by the scalp distributions of waveform-1s, which have large power at the occipital regions (Figs. 7 and 10C).

The early parts (0–300 ms) of waveform-1s in the Go trials resemble those of the stimulus-triggered average EEGs during the Go trials (Fig. 7A). This indicates that, in the early parts (0–300 ms) of the stimulus-triggered average EEGs during the Go trials, the effect of the overlapping of the other waveforms, such as movement-related potentials (MRPs), is small. The effect of the overlapping of MRPs on stimulus-triggered average EEGs during Go trials has been debated (Kok, 1988; Smith et al., 2008; Verleger, 1988; Verleger et al., 2006). With the proposed method, we extracted ourselves from that problem because we can obtain pure waveforms uncontaminated with MRPs.

Waveform-1s in the NoGo trials resemble the stimulus-triggered average EEGs during the NoGo trials (Fig. 10A). This indicates that, in the stimulus-triggered average EEGs during the NoGo trials, the effect of the overlapping of the other waveforms is small. Waveform-1s in the NoGo trials exhibit N200 and P300 as well as the stimulus-triggered average EEGs. The peaks in the waveform-1s in the NoGo trials may reflect the motor inhibition or the detection of the response conflict as discussed for those in the Go/NoGo literature (Bokura et al., 2001; Donkers and van Boxtel, 2004; Falkenstein et al., 1999; Ramautar et al., 2004).

Waveforms time-locked to response onsets

Waveform-2s in the Go trials are response-locked. Therefore, these waveforms are considered to reflect such response-related brain processes as execution of button pushes.

Around 400 ms after the response onsets, waveform-2s in the Go trials have large alpha band oscillations (Fig. 8A, black lines). This fact is confirmed by the amplitude spectra (Fig. 8D, black line) and the time-frequency plots (data not shown). The alpha oscillation after the response onsets may be regarded as the event-related synchronization (ERS) of the alpha band (Neuper and Pfurtscheller, 2001). The ERS of the alpha band may represent a deactivated cortical area or inhibited cortical networks (Neuper and Pfurtscheller, 2001). In contrast to the waveform-2s in the Go trials, the response-triggered average EEGs during the Go trials do not have the ERS of the alpha band (Fig. 8A, red lines). This may indicate that the proposed method extracts the ERS of the alpha band but the response-triggered averaging procedure does not.

Waveforms time-locked to neither stimulus nor response onsets

Waveform-3s in the Go trials and waveform-2s in the NoGo trials are time-locked to neither the stimulus nor the response onsets. Such waveforms have been previously hard to see because of their unknown delays.

Verleger et al. (2005) examined EEGs during choice reaction time tasks by stimulus- and response-triggered averaging procedures and showed evidences that a component (P3b) is time-locked to neither stimulus nor motor response onsets. Like P3b, the positive peaks in the waveform-3s in the Go trials appear around 300 ms after the stimulus onsets and are time-locked to neither the stimulus nor the response onsets. Verleger et al. (2005) suggested that P3b reflects a process that mediates between perceptual analysis and response initiation. It remains unclear whether their interpretation can be applied to the positive peaks in the waveform-3s in the Go trials because the delays of the positive peaks in the waveform-3s are longer than the RTs in about half of the Go trials; if the peaks reflect the mediating process, their delays should be between the stimulus and the response onsets.

On the other hand, the properties (temporal waveforms, delays, scalp distributions, and amplitude spectra) of waveform-3s in the Go trials resemble those of waveform-2s in the NoGo trials (Figs. 9 and 11). This may indicate that these waveforms reflect the same brain process in the Go and NoGo trials, such as monitoring task performance. To elucidate the functional role of the waveforms, we need further examinations, such as a comparison with the waveforms estimated from EEGs during a variety of tasks and a source estimation of the waveforms.

Conclusion

We proposed a generalized method to estimate EEG waveforms common across trials. The main achievement of the proposed method is its ability to deal with an unknown number of multiple waveforms and multi-channel EEGs. In general situations, this method can be used in a variety of ways.

Acknowledgments

This research was supported by a contract with the National Institute of Information and Communications Technology entitled, “Multimodal integration for brain imaging measurements”.

Appendix A

The procedure for random search in global search is described in MATLAB style as follows:

```
Generate τ by random numbers;
Obtain o_τ;
for iter = 1:20
for k = 1:K
 for n = 1:N
  Make τ' by changing τ_{n,k} in τ randomly;
  Obtain o_τ';
  if o_τ' < o_τ
     o_τ = o_τ';
     τ = τ';
  end
    end
  end
end.
```

The procedure for grid search in local search is described in MATLAB style as follows:

Set τ selected in global search;
Obtain o_τ;
$o' = o_\tau + \mathbf{1}$;
while $o_\tau < o'$
  $o' = o_\tau$;
  for $k = 1$:K
for $n = 1$:N
  for t $= \tau_{\min}$:τ_{step}:$\tau_{\max}$
    Make τ' by changing $\tau_{n,k}$ in τ to t;
    Obtain $o_{\tau'}$;
    if $o_{\tau'} < o_\tau$
      $o_\tau = o_{\tau'}$;
      $\tau = \tau'$;
    end
        end
      end
    end
end,

where $\tau_{\min}$: minimum value of $\tau_{n,k}$, τ_{step}: step of $\tau_{n,k}$, and $\tau_{\max}$: maximum value of $\tau_{n,k}$.

References

Akaike, H., 1974. A new look at the statistical model identification. IEEE Trans. Automat. Contr. AC-19 716–723.

Biggins, C.A., MacKay, S., Clark, W., Fein, G., 1997. Event-related potential evidence for frontal cortex effects of chronic cocaine dependence. Biol. Psychiatry 42, 472–485.

Bokura, H., Yamaguchi, S., Kobayashi, S., 2001. Electrophysiological correlates for response inhibition in a Go/NoGo task. Clin. Neurophysiol. 112, 2224–2232.

Braun, C.M.J., Villeneuve, L., Gruzelier, J.H., 2002. Topographical analysis of stimulus-related and response-related electrical scalp activity and interhemispheric dynamics in normal humans. Int. J. Psychophysiol. 46, 109–122.

Donkers, F.C.L., van Boxtel, G.J.M., 2004. The N2 in go/no-go tasks reflects conflict monitoring not response inhibition. Brain Cogn. 56, 165–176.

Endo, H., Kizuka, T., Masuda, T., Takeda, T., 1999. Automatic activation in the human primary motor cortex synchronized with movement preparation. Cogn. Brain Res. 3, 229–239.

Falkenstein, M., Hoormann, J., Hohnsbein, J., 1999. ERP components in Go/Nogo tasks and their relation to inhibition. Acta Psychol. 101, 267–291.

Goodin, D.S., Aminoff, M.J., Mantle, M.M., 1986. Subclasses of event-related potentials: response-locked and stimulus-locked components. Ann. Neurol. 20, 603–609.

Jaśkowski, P., Verleger, R., 1999. Amplitudes and latencies of single-trial ERP's estimated by a maximum-likelihood method. IEEE Trans. Biomed. Eng. 46, 987–993.

Jaśkowski, P., Verleger, R., 2000. An evaluation of methods for single-trial estimation of P3 latency. Psychophysiol 37, 153–162.

Jung, T.-P., Makeig, S., Westerfield, M., Townsend, J., Courchesne, E., Sejnowski, T.J., 2001. Analysis and visualization of single-trial event-related potentials. Hum. Brain Mapp. 14, 166–185.

Kok, A., 1988. Overlap between P300 and movement-related-potentials: a response to Verleger. Biol. Psychol. 27, 51–58.

Makeig, S., Delorme, A., Westerfield, M., Jung, T.-P., Townsend, J., Courchesne, E., Sejnowski, T.J., 2004. Electroencephalographic brain dynamics following manually responded visual targets. PLoS Biol. 2, 0747–0762.

McGillem, C.D., Aunon, J.I., Pomalaza, C.A., 1985. Improved waveform estimation procedures for event-related potentials. IEEE Trans. Biomed. Eng. 32, 371–379.

Mihaylova, M., Stomonyakov, V., Vassilev, A., 1999. Peripheral and central delay in processing high spatial frequencies: reaction time and VEP latency studies. Vision Res. 39, 699–705.

Möcks, J., Köhler, W., Gasser, T., Pham, D.T., 1988. Novel approaches to the problem of latency jitter. Psychophysiol 25, 217–226.

Neuper, C., Pfurtscheller, G., 2001. Event-related dynamics of cortical rhythms: frequency-specific features and functional correlates. Int. J. Psychophysiol. 43, 41–58.

Pham, D.T., Möcks, J., Köhler, W., Gasser, T., 1987. Variable latencies of noisy signals: estimation and testing in brain potential data. Biometrika 74, 525–533.

Puce, A., Berkovic, S.F., Cadusch, P.J., Bladin, P.F., 1994a. P3 latency jitter assessed using 2 techniques: I. Simulated data and surface recordings in normal subjects. Electroencephalogr. Clin. Neurophysiol. 92, 352–364.

Puce, A., Berkovic, S.F., Cadusch, P.J., Bladin, P.F., 1994b. P3 latency jitter assessed using 2 techniques: II. Surface and sphenoidal recordings in subjects with focal epilepsy. Electroencephalogr. Clin. Neurophysiol. 92, 555–567.

Ramautar, J.R., Kok, A., Ridderinkhof, K.R., 2004. Effects of stop-signal probability in the stop-signal paradigm: the N2/P3 complex further validated. Brain Cogn. 56, 234–252.

Smith, J.L., Johnstone, S.J., Barry, R.J., 2008. Movement-related potentials in the Go/NoGo task: the P3 reflects both cognitive and motor inhibition. Clin. Neurophysiol. 119, 704–714.

Takeda, Y., Yamanaka, K., Yamamoto, Y., 2008a. Temporal decomposition of EEG during a simple reaction time task into stimulus- and response-locked components. NeuroImage 39, 742–754.

Takeda, Y., Yamanaka, K., Nozaki, D., Yamamoto, Y., 2008b. Extracting a stimulus-unlocked component from EEG during NoGo trials of a Go/NoGo task. NeuroImage 41, 777–788.

Tallon-Baudry, C., Bertrand, O., 1999. Oscillatory gamma activity in humans and its role in object representation. Trends Cogn. Sci. 3, 151–162.

Vassilev, A., Mihaylova, M., Bonnet, C., 2002. On the delay in processing high spatial frequency visual information: reaction time and VEP latency study of the effect of local intensity of stimulation. Vision Res. 42, 851–864.

Vaughan Jr., H.G., Costa, L.D., Gilden, L., 1966. The functional relation of visual evoked response and reaction time to stimulus intensity. Vision Res. 6, 645–656.

Verleger, R., 1988. The true P3 is hard to see: some comments on Kok's (1986) paper on degraded stimuli. Biol. Psychol. 27, 45–50.

Verleger, R., Jaśkowski, P., Wascher, E., 2005. Evidence for an integrative role of P3b in linking reaction to perception. J. Psychophysiol. 19, 165–181.

Verleger, R., Paehge, T., Kolev, V., Yordanova, J., Jaśkowski, P., 2006. On the relation of movement-related potentials to the go/no-go effect on P3. Biol. Psychol. 73, 298–313.

Woody, C.D., 1967. Characterization of an adaptive filter for the analysis of variable latency neuroelectric signals. Med. Biol. Eng. 5, 539–553.

Zhigljavsky, A.A., 1991. Theory of Global Random Search. Kluwer Academic Publishers.